AN ANALYSIS OF THE TOPEX/POSEIDON OPERATIONAL ORBIT: OBSERVED VARIATIONS AND WHY

Raymond B. Frauenholz
Ramachandra S. Bhat
Bruce E. Shapiro

Jet Propulsion Laboratory
California Institute of Technology
Pasadena, California

Robert K. Leavitt

Sterling Software, Inc.
Pasadena, California

AAS/AIAA Astrodynamics Specialist Conference

HALIFAX, NOVA SCOTIA, CANADA   14–17 AUGUST 1995

An Analysis of the TOPEX/Poseidon Operational Orbit: Observed Variations and Why[*]

R. B. Frauenholz[+], R. S. Bhat[#] and B. E. Shapiro[#]

Jet Propulsion Laboratory, California Institute of Technology, Pasadena, Ca.

R. K. Leavitt,[**]

Sterling Software, Inc., Pasadena, Ca.

Introduction

Following its launch on 10 August 1992, TOPEX/Poseidon began and continues a very successful global study of the earth's ocean circulation using a combination of dual-frequency radar altimetry and precision orbit determination. Having recently completed the primary three-year mission, this joint project of NASA and the French Space Agency CNES (*Centre National d'Etudes Spatiales*) has now begun a three-year extended mission phase.

Precision orbit determination (POD) performed by the Goddard Space Flight Center (GSFC) using laser ranging measurements and data acquired by the CNES tracking system DORIS (Doppler Orbitography and Radiopositioning Integrated by Satellite) defines radial position relative to the geocenter to an unprecedented accuracy of ~5 cm rms.[1] The POD results are utilized here to reconstruct the operational orbit history in terms of precise classical mean elements. This paper describes the method used to compute mean elements, establishes their accuracies, and identifies the major perturbing forces affecting their variation and the 10-day repeat ground track.

Operational Orbit

Early TOPEX/Poseidon mission and orbit design investigations by Frautnick and Cutting[2] identified the need for accurate control of an exactly repeating satellite ground track to meet science objectives. Farless[3] later defined a detailed orbit design space from which the operational orbit was ultimately selected. The reference orbit provides an exact repeat ground track covering 127 orbits over 10 sidereal days, phased to also overfly two verification sites to facilitate altimeter calibration activities during the first six months.

The reference mean elements presented in Table 1 provide a near-circular frozen orbit at a mean altitude of ~1336 km and an inclination of ~66 deg. Use of a frozen orbit restricts the variation in orbit eccentricity and argument of periapse to limit satellite altitude variability for enhanced altimetry performance, while also eliminating the need for dedicated maneuvers to control these parameters. The semimajor axis a_o and inclination i_o define a reference ground track with a 10-day repeat cycle and precise overflight of the altimeter verification sites. This tuning process requires a 20x20 gravity field to provide a frozen orbit, defined by the mean eccentricity e_o and argument of periapse ω_o values listed in Table 1.

Table 1. Reference Mean Elements and Orbit Determination Requirements for the Operational Orbit

Orbital Parameters	Reference Value	3σ Orbit Determination Requirement
Semimajor Axis a_o (km)	7714.42938	1 meter
Inclination i_o (deg)	66.0408	0.1 mdeg
Eccentricity e_o (ppm)	95	5 ppm
Argument of Periapse ω_o (deg)	90	20 deg

Periodic orbit maintenance maneuvers (OMMs) adjust the mean semimajor axis to keep the ground track within ±1 km of the repeating reference track in the presence of all perturbations, while also ensuring that other orbital parameters remain within required limits. Maintaining $e \leq 0.001$ provides desired orbital altitude control; use of a frozen orbit assures the mean eccentricity remains an order of magnitude smaller without dedicated maneuvers. Inclination variations of ~3 mdeg about the reference mean value i_o assures required ground track control without the need for inclination corrections. Effective ground track control requires an accurate method of computing these mean orbital parameters.


Mean Orbital Elements

Guinn[4] developed an osculating-to-mean element conversion technique consistent with the stringent ±1-km ground track control requirements. Guinn's conversion method allows removal of all central body zonal, sectorial, and tesseral harmonics, second-order J_2, and third-body perturbations acting over a specified time interval. Usually, longitude-dependent gravity terms lead to periodic effects which average to near-zero over a day. However, such cancellation does not result when the satellite motion is nearly commensurate with earth rotation as occurs when the satellite orbit repeats relative to the rotating earth. Instead, resonances arise when the satellite completes β nodal periods while the earth rotates α times relative to the *precessing* satellite orbit plane. The TOPEX/Poseidon ground track repeats every 127 orbits over ~10 days, so $\beta/\alpha \approx 127/10$. Gravity terms that are near-multiples of this β/α ratio contribute secular forces. The first- and second-order near-resonant terms are included in truncated 13x13 and 26x26 gravity fields. The importance of these near-resonant terms to osculating-to-mean element conversion depends on the specific accuracy requirements.

Semimajor axis accuracy is of primary importance to effective ground track control. The required determination accuracy of one meter (3σ) is provided by the GSFC Flight Dynamics Facility (FDF) using one-way Doppler acquired via the NASA Tracking and Data Relay Satellite System (TDRSS).[5] The 3σ accuracy requirements placed on the FDF for determination of eccentricity e, inclination i, and argument of periapse ω are listed in Table 1.

Fig. 1 describes the osculating-to-mean element conversion accuracy as a function of gravity field size while removing all periodic gravitational perturbations acting over 10 days, the duration of one ground track repeat cycle. Accuracy is measured relative to a "truth" gravity model, defined from a 26x26 truncation of the 70x70 JGM2 model obtained by post-launch POD.[1] Use of this truth model includes the effects of second-order resonances. The semimajor axis requires a 20x20 gravity field to reduce mean element computational errors to a negligible level, whereas the other orbital parameters achieve satisfactory accuracy using smaller gravity fields (Fig. 1b).
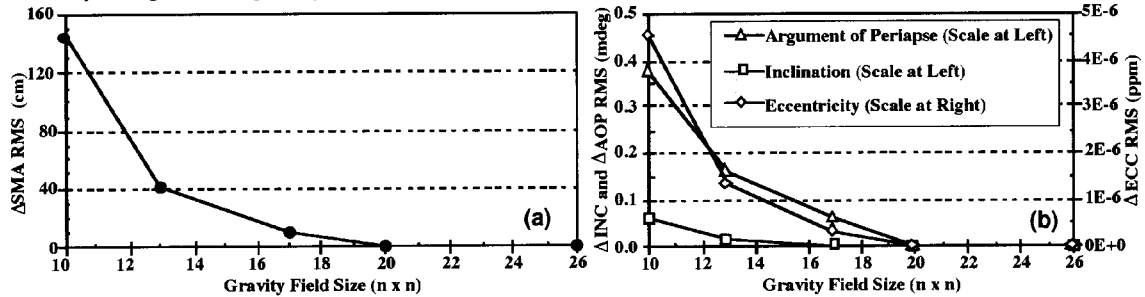

**Fig. 1. Mean Element Computation Accuracy Relative to 26x26 Gravity Field
(Includes Removal of Third-Body Gravity Perturbations over 10 days)**

To measure long-term stability characteristics of the mean element conversion process, mean semimajor axis values were computed every 28 min (about every quarter orbit) from POD ephemerides (POEs) for the 20-day period from 3 to 23 March 1994 (repeat cycles 54 and 55). Fig. 2 compares the mean semimajor axis values obtained using 2x2, 10x10, 13x13, 17x17, and 20x20 gravity field sizes with values obtained from the 26x26 "truth" model. The differences of each case from the truth are consistently unbiased across the 20-day comparison interval with a periodicity similar to the 10-day ground track repeat cycle. Fig. 2(a) compares the osculating semimajor axis with the mean values obtained by removing earth oblateness present in the 2x2 gravity terms. The osculating values vary ±7.2 km about the truth mean, whereas the amplitude of this variation reduces to ±80 meters by removing oblateness. Removing perturbations of the 10x10 gravity field reduces the amplitude to ±3.6 meters. The amplitude of the computational errors drops to ±130 cm by removal of the first-order resonances present in the 13x13 gravity field. The error envelope reduces further to ±33 cm by increasing the gravity field to 17x17, and to a negligibly small ±1 cm using the 20x20 gravity field.

2
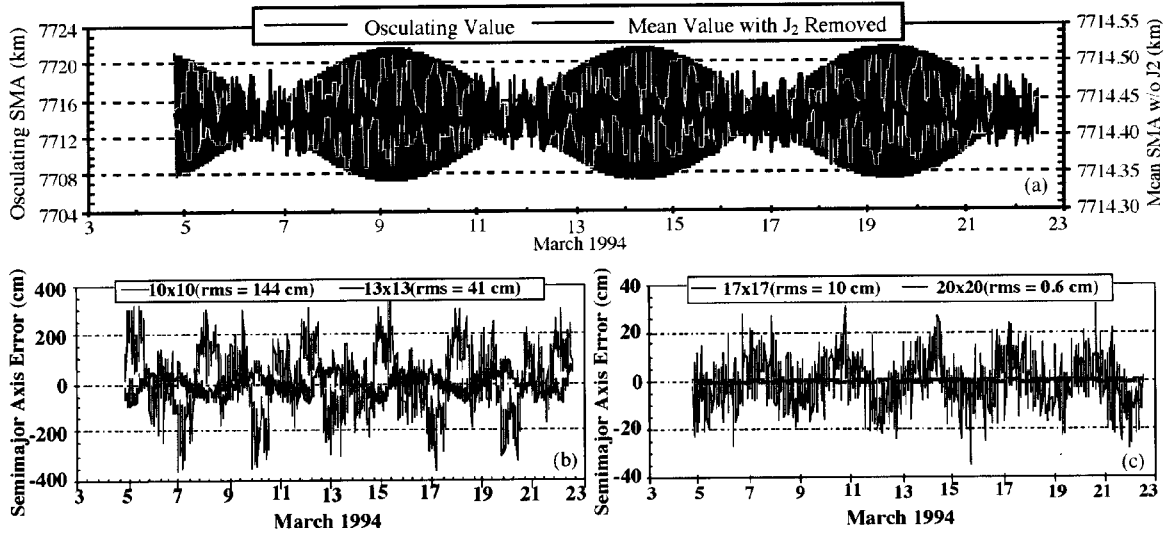
Fig. 2. Mean Semimajor Axis Computation Accuracy Relative to 26x26 Gravity Field
(Removal of Geopotential and Third-Body Gravity Perturbations Acting Over 10 days)

The results presented in Figs. 1 and 2 indicated removal of all perturbations present in a 20x20 gravity field acting over 10 days provided stable values of the mean semimajor axis. Fig. 3 summarizes the effects of removing these perturbations over periods less than 10 days. In Fig. 3(a), removal of perturbations acting over just one orbital period (~112 min) results in mean semimajor axis computational errors of ±3 meters. Removal of these perturbations over one, three, and five days shown in Fig. 3(b) reduces these errors to ±20 cm, ±10 cm, and to identically zero, respectively. Further review of the osculating semimajor axis presented in Fig. 1 reveals two sinusoidal trends, each with a 10-day period, but out of phase by 180 deg. This behavior allows mean semimajor axis for this orbit to be accurately determined by removing central and third-body perturbations with periods that are any multiple of five days. For convenience, 10 days has been selected to synchronize with the ground track repeat frequency.
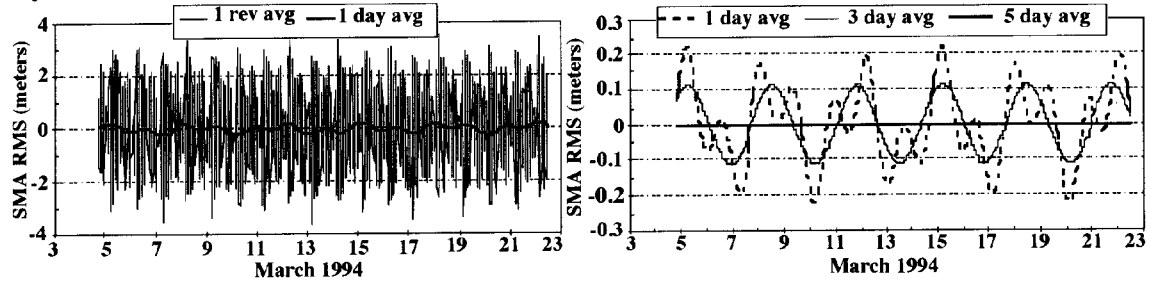
Fig. 3. Effect of Perturbation Removal Interval on Mean Semimajor Axis Computation
Accuracy for 20x20 Gravity Field (Includes Removal of Third-Body Gravity Perturbations)
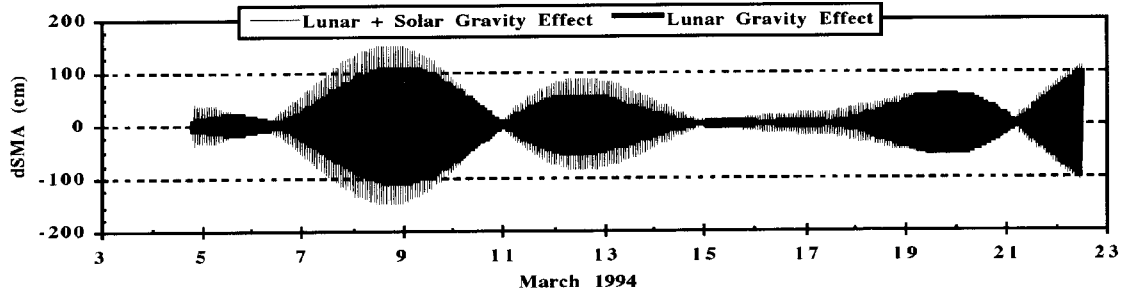
Fig. 4. Effects of Lunar and Solar Gravity on Mean Semimajor Axis Computation Accuracy

3

The individual effects of lunar and solar gravity on the computational accuracy of mean semimajor axis are presented in Fig. 4. The reference for comparison is computed by removing central (20x20) and third-body gravitational perturbations acting over 10 days. Ignoring the third-body perturbations results in mean semimajor axis errors as large as ±150 cm for the interval shown. However, these comparisons indicate that lunar gravity is by far the dominant force.

Based on the foregoing analyses, mean orbital elements for TOPEX/Poseidon are computed by removing all central and third-body perturbations acting over 10 days. Use of a 20x20 gravity field provides the one-sigma mean element computational accuracies listed in Table 2.

Table 2. Mean Orbital Element Computational Accuracies

Orbital Parameters	Reference Value	1σ Computational Accuracy
Semimajor Axis a_o (km)	7714.42938	13 cm
Inclination i_o (deg)	66.0408	0.5 mdeg
Eccentricity e_o (ppm)	95	7 ppm
Argument of Periapse ω_o (deg)	90	9 deg

Semimajor Axis

Pre-launch studies[6] indicated ground track control could be effectively provided by periodic removal of accumulated semimajor axis decay caused by along-track forces due almost entirely to atmospheric drag. The rate of semimajor axis decay of this near-circular orbit was expected to depend primarily on the 81-day mean $F_{10.7}$ solar flux.[7] At launch in August 1992, the mean solar flux was $\sim 125 \times 10^{-22}$ watts/m^2/Hz and has steadily declined as the minimum of solar cycle 22 approaches, currently expected in late 1996.

The semimajor axis decay rate induced by drag (Eq. 1) is primarily a function of the solar flux level and the satellite area-to-mass ratio (A/m). TOPEX/Poseidon uses sinusoidal yaw steering and fixed yaw control modes to maintain nadir pointing for altimetry and to keep the large 28 m^2 solar array (SA) pointed near the sun for power management. While executing these attitude control strategies, the satellite area projected in the along-track direction, and affecting drag, varies continuously between the extremes of ~ 9 m^2 and ~ 22 m^2. As a result, the A/m of the 2406-kg satellite varies between ~ 0.004 and ~ 0.009 m^2/kg. Fig. 5 shows the semimajor axis decay rate as a function of the 81-day mean solar flux for these two A/m extremes. For solar flux levels less than ~ 125 experienced by TOPEX/Poseidon, the decay rates due to drag are generally low, varying between ~ 1 and ~ 7 cm/day.

$$\frac{da}{dt} = -\rho C_D \frac{A}{m} \sqrt{\mu a} \left[1 - \frac{\omega_e \cos i}{n} \right]^2$$

where ρ = atmospheric density, primarily a function solar flux

C_D = satellite drag coefficient

A/m = satellite area - to - mass ratio, varies with yaw control mode

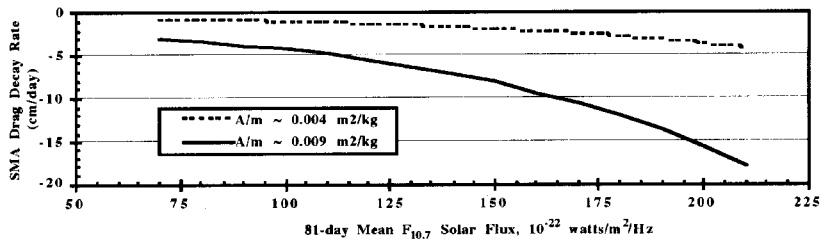μ = central body gravitational constant   (1)

a = orbit mean semimajor axis

ω_e = earth rotation rate

i = orbit mean inclination

$n = \sqrt{\mu/a^3}$, the orbit mean motion

Fig. 5. Predicted Semimajor Axis Decay Rate Due to Drag

4

Observed Semimajor Axis

Fig. 6 shows the mean semimajor axis history after achieving the operational orbit in September 1992 until just prior to OMM8 on 22 May 1995. Each of the eight OMMs raised the semimajor axis above the reference value a_o (Table 1) to reverse the satellite ground track westward and thereby remain within the ±1-km control band (shown later in Fig. 20). This process requires maneuvers on the order of 3 to 4 mm/s applied in the along-track direction (note that $dV/da \cong 0.466$ mm/s per meter for this orbit).

The expected monotonic decay in semimajor axis was not always observed. Instead, the semimajor axis sometimes increased, suggesting the presence of additional along-track forces, now confirmed to have body-fixed origins.[8] Although a credible physical model for their behavior remains to be more fully developed, these body-fixed forces arise from the combined effects of solar radiation, thermal gradients, and molecular outgassing, produced mostly by the large SA, particularly during a fixed yaw mode. These persistent forces cause either orbital boost or deboost, depending on the satellite yaw control mode.[8]
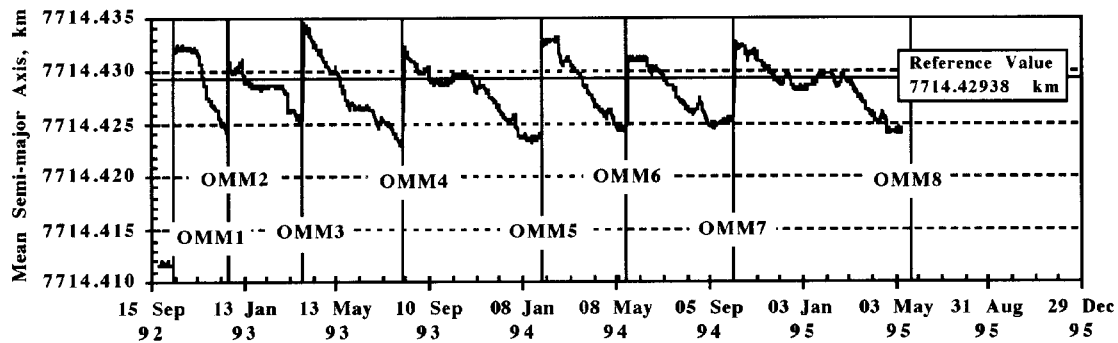

Fig. 6. Mean Semimajor Axis History Based on POD and 20x20 Gravity Field

Shortly before launch, a plan was adopted to use a pitch bias to off-point the SA from the solar-normal to limit peak battery charge currents during each exit from earth occultation. The use of a pitch bias (currently 54 deg) effectively regulates battery performance, but radiation forces normal to the SA are not along the sunline as originally planned and reflected throughout navigation software. As a result, sizable unplanned along-track forces accumulate; the magnitude and direction depend on the specific yaw control mode. These body-fixed forces can either offset or add to the ever-present decay in semimajor axis induced by atmospheric drag. Estimates of these forces and an effective prediction model were needed to more confidently monitor semimajor axis behavior and to maintain the satellite ground track.

Atmospheric Drag and Body-Fixed Forces

The combined effects of atmospheric drag and the body-fixed forces on semimajor axis have been effectively estimated from daily quick-look orbit determination solutions based on precise laser ranging measurements.[9] A byproduct of this process is the total once/rev along-track non-gravitational acceleration from which the total rate of change in semimajor axis can be easily computed.* Isolation of the body-fixed forces then requires removal of the drag contributions. The integrity of this process depends on the accuracy of the atmospheric density model, and this always raises reasonable concern. Operational navigation tasks reported here have been performed using the Jacchia-Roberts[10-13](JR) density model. Drag forces computed with the JR density model are compared with those predicted by the Drag Temperature Model[14](DTM), although neither model reflects flight data at the TOPEX/Poseidon altitude.

The yaw steering period from 6 March to 24 April 1994, included in Fig. 6, shows the semimajor axis generally exhibited the intuitive monotonic "drag-like" decay behavior; the net decay rate was ~11.7 cm/day. Fig. 7 shows daily quick-look laser ranging estimates of the total decay rate due to all non-gravitational forces varies with the β' angle,+ varying between -10 and -15 cm/day. However, the decay rate

---

* An along-track acceleration of one nanometer/sec^2 induces a rate of change in semimajor axis of 18.5 cm/day.

+ β' is the angle between the orbit plane and the geocentric direction to the sun.

5

induced by atmospheric drag alone is much less, varying between -2 and -5 cm/day for both the JR and DTM density models, as the 81-day mean solar flux steadily dropped from ~100 to ~80. Removing the drag effects from the total decay rate provides estimates of the body-fixed contribution. In this example, the body-fixed and drag-induced forces are of similar magnitude at lower values of β', whereas the body-fixed forces dominate at higher β', especially when the orbit is in full sun ($\beta' > 55.7$ deg).

Fig. 8 presents the empirical model defining changes in mean semimajor axis induced by the body-fixed forces. The model defines these changes in terms of a polynomial function of the β' angle which has a periodic variation of ~112 days. The satellite executes sinusoidal yaw steering outside the nominal limits of $-15 \le \beta' \le 15$ deg; within these β' limits fixed yaw modes are used. A 180-deg yaw flip maneuver near $\beta'=0$ deg keeps the SA on the satellite sunlit side. Using these yaw control modes the body-fixed forces cause either orbital boost or deboost, either increasing or decreasing the mean semimajor axis. Sometimes the body-fixed forces add to the ever-present decay due to drag, and sometimes they offset the effects of drag. In either case, the net effects on the semimajor axis and satellite ground track must be determined by dynamically summing these individual forces.
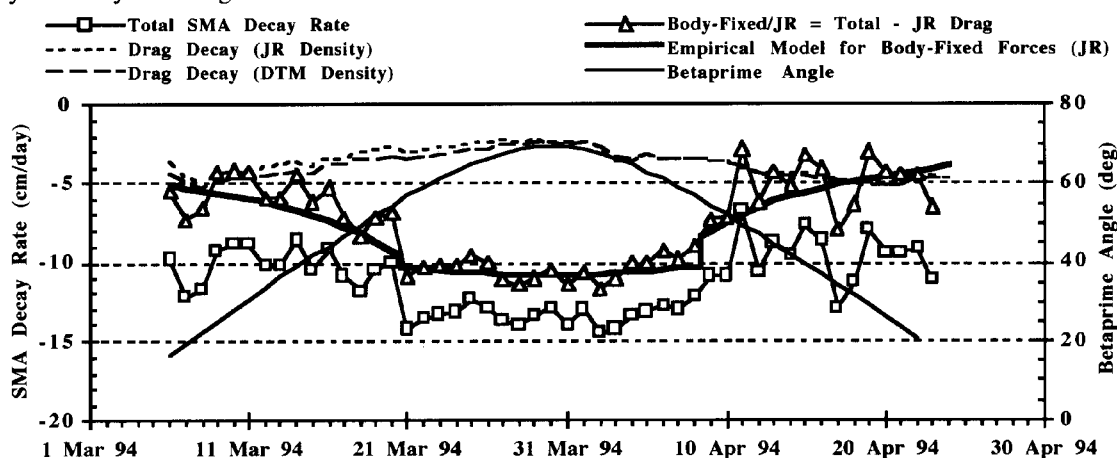

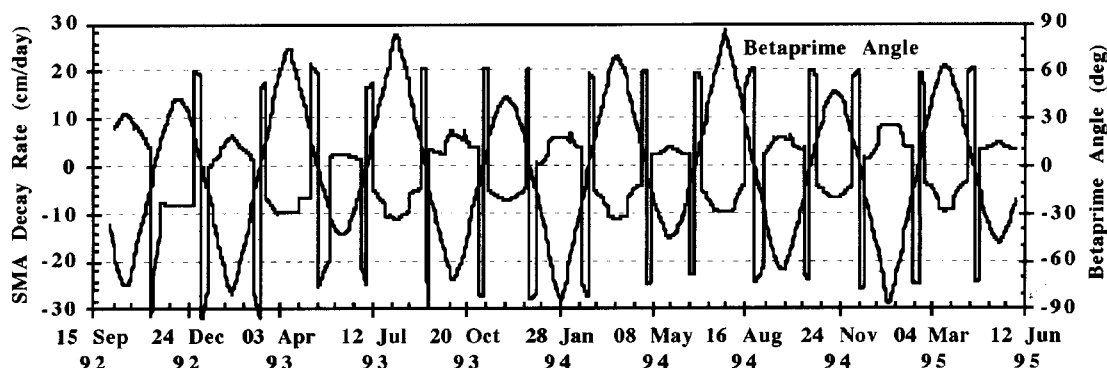Fig. 7. Total Semimajor Axis Decay Rate due to Non-Gravitational Forces

Fig. 8. Semimajor Axis Decay Rate due to Body-fixed Forces

Over the course of the mission, Richter[15-17] has evolved theoretical models of the body-fixed forces for each yaw control mode using estimates of satellite surface properties and inflight temperature measurements. Differences between the theoretical models and observations are currently most notable during yaw steering, especially while transitioning to and from full sun when uncertain SA curling responses induced by thermal imbalances are believed to be the primary contributors to the observed along-track forces. Ongoing improvements in the theoretical models may eventually permit their operational use instead of the more complex and tedious empirical techniques currently required. Such modeling

improvements may simplify flight operations and eventually allow more confident isolation of drag contributions that could lead to improved density models.

Effect of Body-Fixed Forces on Mean Semimajor Axis and the Satellite Ground Track

The effect of the body-fixed forces on the semimajor axis and satellite ground track were assessed during March 1994 (when $\beta' > 0$) by comparing two precision integrated trajectories, one with all known force models active, the other with only the body-fixed forces turned off. Fig. 9 shows the resulting semimajor axis values; Fig. 10 then isolates these effects on the ground track. When all force models are active, the semimajor axis first exhibits boost, followed by a sustained period of deboost at a nearly-linear rate of -11.7 cm/day. When the body-fixed forces are removed the overall deboost rate drops substantially to only -4.3 cm/day. This remaining force is attributed to just atmospheric drag. Earlier (Fig. 7), the decay rates due to drag were estimated analytically for both the JR and DTM density models based on daily solar flux observations. These results are also shown in Fig. 9 for direct comparison with the two semimajor axis deboost trends. The decay due to drag drops from ~5 to ~3 cm/day as the 81-day mean solar flux drops from ~100 to ~80 during the comparison period. The average value of -4 cm/day agrees favorably with the drag effects estimated from the slope of the semimajor axis, confirming that body-fixed forces and atmospheric drag are the primary sources of observed semimajor axis decay.
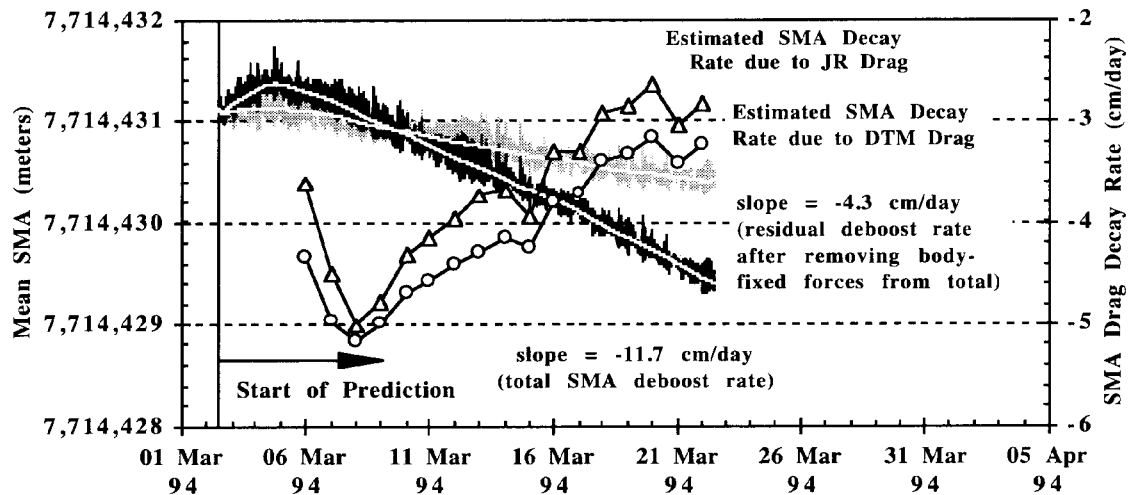

Fig. 9. Effects of Body-Fixed Forces and Drag on the Mean Semimajor Axis
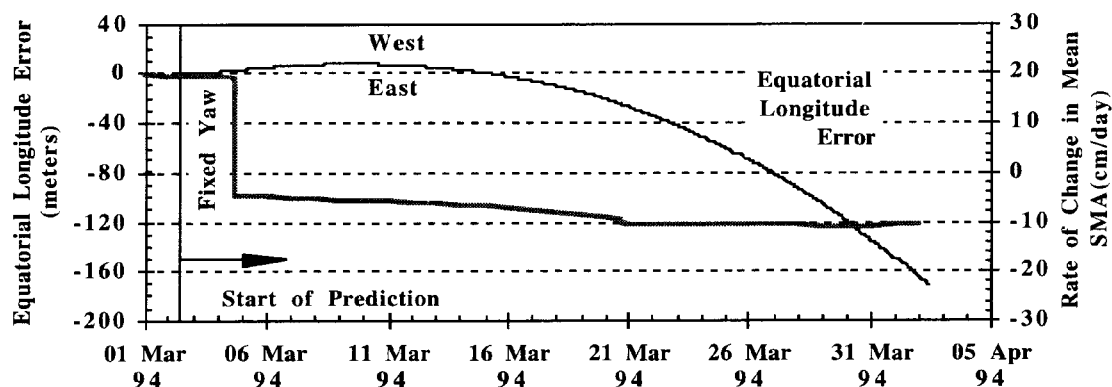

Fig. 10. Effects of Body-Fixed Forces on the Satellite Ground Track

Changes in the satellite ground track due to the body-fixed forces are shown in Fig. 10 in terms of equatorial longitude differences. The comparison starts during a fixed yaw mode when the body-fixed

forces induce an orbital boost rate of ~20 cm/day. When the satellite resumes yaw steering, the body-fixed forces abruptly change in both magnitude and direction, initially causing a semimajor axis deboost rate of ~5 cm/day, gradually increasing to ~10 cm/day as the β' angle increases. When these body-fixed forces are turned off, the orbital boost forces active at the beginning of the prediction interval cause the ground track to initially drift eastward. After resuming yaw steering, the accumulated effect of removing the deboost forces causes the ground track to drift increasingly westward. For this example, the net integrated effect on the satellite ground track becomes significant: ~120 meters after 30 days.

Effect of Solar Radiation Pressure on the Mean Semimajor Axis

Solar radiation pressure has only modest effects on the semimajor axis and ground track because its influence averages to near-zero when the orbit is in full sun ($\beta' > 55.7$ deg); the net effect during occultation periods is quite small compared to other perturbing forces. While of secondary interest in this ground track control problem, the effects of solar radiation pressure have been included for completeness. Fig. 11 shows the change in semimajor axis for the six-month period beginning on 1 March 1994. Computed daily, differences in the mean semimajor axis exhibit periodic behavior with peak amplitudes less than ±15 cm. The smallest errors occur during peak β' when the orbit is in full sun; the maximum errors occur near $\beta' = 0$ when the occultation intervals are greatest.
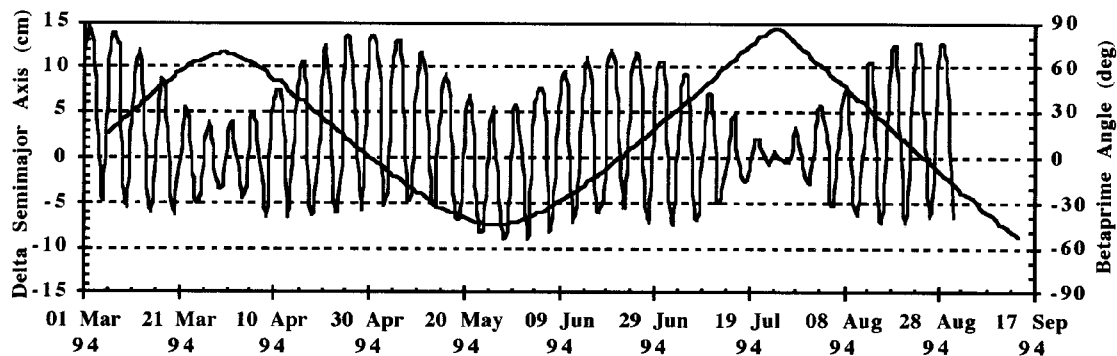

Fig. 11. Effects of Solar Radiation Pressure on Mean Semimajor Axis

Inclination

The mean inclination angle for the TOPEX/Poseidon reference orbit (Table 1) is a direct byproduct of the orbit and ground track design process described earlier. To maintain the repeating orbit and verification site overflights, it is necessary that the inclination remains very close to the reference value (Table 1). Pre-launch analyses[6] indicated that gravitational perturbations due to the sun and moon cause periodic variations in inclination, expected to vary ±3.8 mdeg about the reference value. These analyses also indicated that inclination variations are negligible for non-gravitational perturbations such as solar radiation pressure and atmospheric drag. The ground track targeting procedure absorbs these inclination variations by suitably adjusting the mean semimajor axis to maintain the repeating ground track within ±1 km, thereby eliminating the need for inclination corrections during the three-year prime mission.
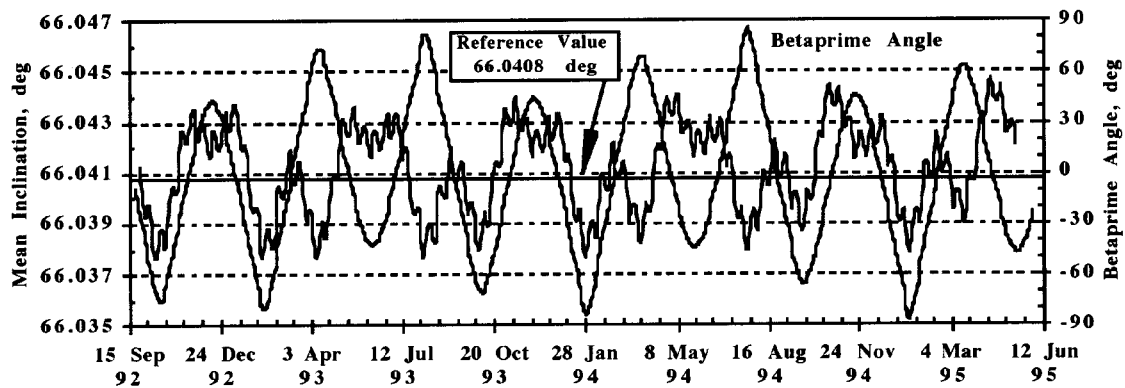
Observed Variations of Inclination

Since first achieving the operational orbit in September 1992, the observed mean inclination has exhibited the expected periodic variations about the reference value. During 1992, the peak amplitudes of these variations were -3.3 mdeg and +3.0 mdeg; more recently these amplitudes have shifted positively to -2.7 mdeg and +3.7 mdeg. These variations are a combination of several clearly distinguishable periodic components of 12, 58, and 173 days. There are also very long periodic variations which have become noticeable after three years, but these amplitudes appear to be quite small. Pre-launch analyses indicated that the major components are due to third-body gravitational perturbations. Table 3 lists the amplitude and period of these perturbations. Fig. 12 shows that the inclination variation about the reference value correlates very well with the β' angle, as does the amplitude of the periodic components. The amplitudes are higher when the orbit is in full sun ($\beta' > 55.7$ deg), while the mean inclination is always greater than the reference value during occultation periods.

8

Eight OMMs have been implemented since September 1992. These small maneuvers (3 to 5 mm/s), applied in the along-track direction to raise semimajor axis, have had a negligible effect on the orbit inclination. Only unplanned cross-track components could affect inclination, but these velocity magnitude errors are extremely small (note that $dV/di \approx 125$ mm/s per mdeg applied normal to the orbit plane).

Table 3. Periodic Inclination Variations due to the Sun and Moon Gravitational Perturbations

Perturbing Force	Amplitude (mdeg)	Period of Variation (days)
Lunar Gravity	0.098	12.56
	1.325	173.40
	0.542	11.72
	0.277	86.70
Solar Gravity	0.354	88.93
	0.660	173.30
	0.582	3402.00
	1.241	58.77 (half of β')
	0.158	86.70

Fig. 12. Observed Orbital Inclination Angle

The observed or definitive inclination includes variations due to both modeled and unmodeled perturbing forces. The behavior is predictable when unmodeled perturbations have a negligible effect. Precision trajectory propagation software with all known models active was used to generate a six-month trajectory beginning 1 March 1994. The predicted inclination was compared over this period with the definitive inclination defined by POD. Fig. 13 shows inclination differences are quite small, indicating the important models are well known and the resulting inclination variations are predictable.
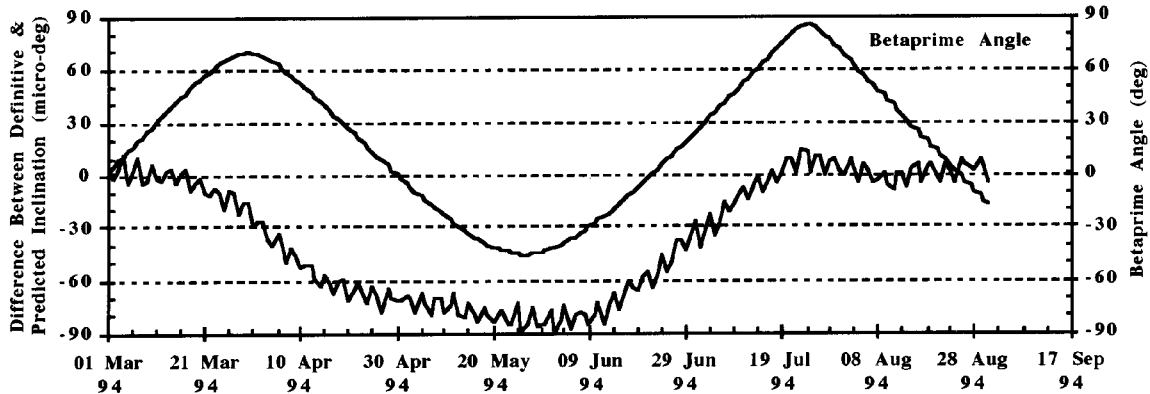
**Fig. 13. Difference Between Definitive and Predicted Inclination**

Perturbation Analyses

Fig. 13 established that the observed inclination variations are predictable and attributable to known modeled perturbations. A detailed analysis established the contributions of each perturbing force using precision trajectory software to generate individual trajectories covering the six-month period beginning 1 March 1994. Inclination variations due to each perturbing force were determined by turning individual models off and comparing the resulting trajectory parameters with the reference case with all models active. The corresponding mean elements were differenced to isolate inclination variations.

Sun and Moon Gravitational Attraction

Pre-launch studies[6] assessed the effect of third-body gravitational perturbations on the satellite ground track from which the inclination variations were also established. The initial analysis was conducted analytically to determine the individual effects of the sun and moon and then verified using precision integrated trajectories.

The inclination variations due to lunar gravity are dominated by the 173-day and 12-day periodic components (Fig. 14, Table 2). However, closer inspection indicates that there are also other significant periodic variations. Analytical studies established the amplitudes and periods of four distinct components; two have amplitudes of ~0.1 and ~0.54 mdeg, with periods 12.6 and 11.7 days, respectively. These two variations appear as a single perturbation in Fig. 14. The amplitude of the 173-day periodic component is 1.33 mdeg; the other periodic component has an 87-day period and a 0.3-mdeg amplitude.
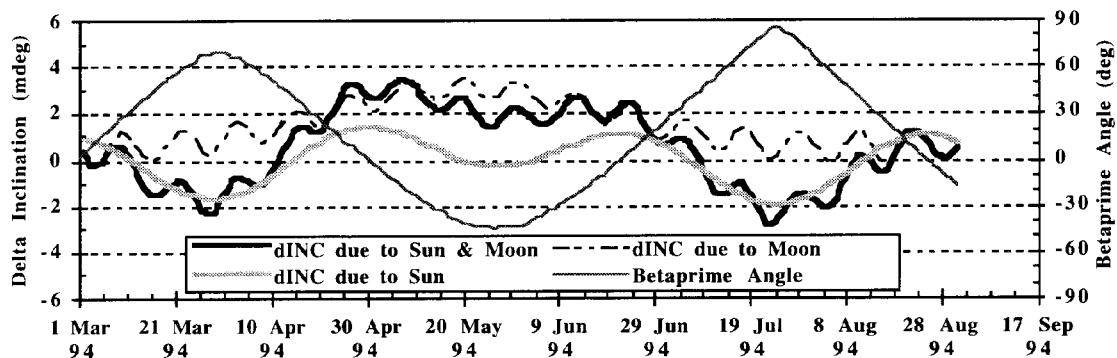
Fig. 14. Inclination Variations due to Lunar and Solar Gravitational Perturbations

There are five significant periodic components in the inclination variation due to solar gravity. These variations are synchronized with the β' angle (Fig. 14). The dominant component has an amplitude of 1.24 mdeg and a period of 58 days, about half the period of β'. One component has a period of 173 days, ~1.5 times the β' period, and an amplitude of 0.66 mdeg. Two components have periods of ~87 days, or about three-quarters of the β' period, with amplitudes 0.35 and 0.16 mdeg, respectively. The fifth component has a period of 9.3 years with an amplitude of 0.58 mdeg. The influence of this component became evident only after two years of mission operations (Fig. 12).

The size and shape of inclination variations due to both the sun and moon are almost identical to the observed variations (Figs. 12, 14), indicating these third-body forces are the primary source of inclination variations. Between March and August 1994, the mean inclination varied between -3 mdeg and +3.5 mdeg due to third-body gravitational perturbations. The amplitude of these variations increases with β', as some of the periodic variations increase when β' is higher.

Effects of Solid Earth Tides and Solar Radiation Pressure

The tidal forces induced by lunar and solar gravity cause small variations in inclination. However, these variations become significant when considering the stringent TOPEX/Poseidon ground track control requirements. The tidal effects are almost an order of magnitude smaller than the third-body gravitational perturbations, but the signature is almost identical and a strong function of the β' angle. Fig. 15 shows the magnitude of the tidal effects varies between -0.4 and +0.3 mdeg between March and August 1994.

10

The inclination variation due to direct solar radiation pressure is very small, and for all practical purposes may be neglected. However, these variations are only a function of the β' angle, shown in Fig. 15 to increase with β'. However, during full-sun periods the variations remain constant; the magnitude is a function of the peak β'. The period of variation (56 to 59 days) is half the β' period; the amplitude was < 0.08 mdeg between March and August 1994.
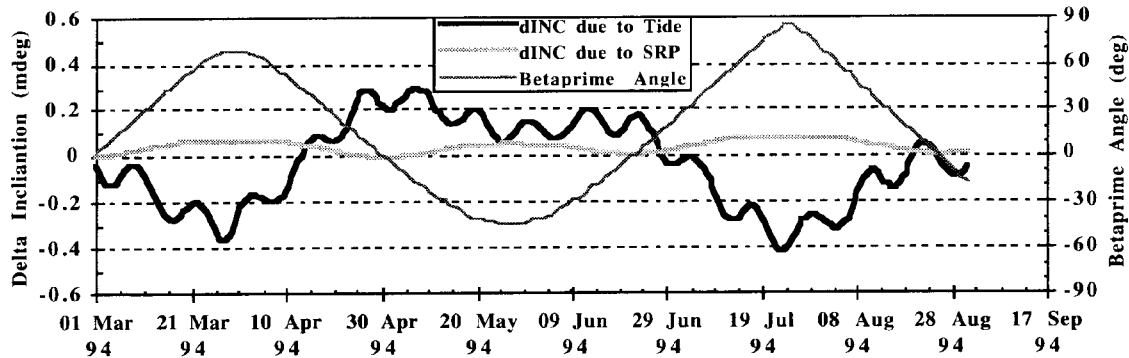

Fig. 15. Inclination Variations due to Tides and Solar Radiation Pressure

Other Forces

The inclination variations due to non-gravitational forces such as atmospheric drag and body-fixed forces are negligible. The rotating atmosphere has some effect on inclination, but negligible compared to variations induced by lunar and solar gravitational perturbations.

Effect of Inclination Variations on the Ground Track

The deviation of inclination from the reference value affects the ground track in two ways. The equatorial crossing slowly deviates due to variations in inclination. The nodal period is a function of inclination. A one-mdeg deviation in inclination changes equatorial crossings by ~280 meters after a 30-day ground track prediction.[18] The maneuver targeting process accounts for inclination-induced variations in ground track prediction and adjusts semimajor axis accordingly so that future nodal crossings remain within the required ±1-km control limit. This process requires predicting the ground track for several months after each maneuver (e.g., Fig. 16). However, the signature of inclination variations is clearly reflected in the ground track, particularly when the mean semimajor axis is within a few meters of the reference value (Table 1). This situation reduces the ground track drift rate relative to the reference track, nominally occurring when the ground track nears the western control boundary (e.g., Fig. 20).
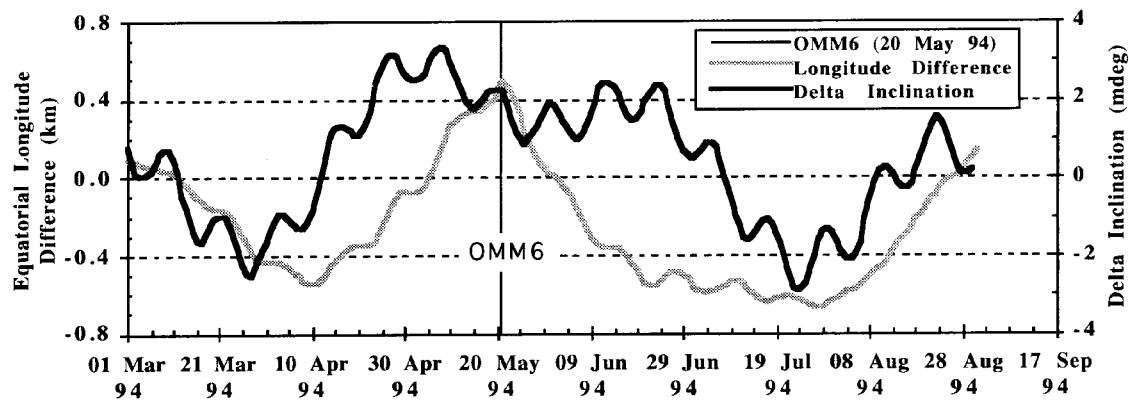

Fig. 16. Comparison of Ground Track and Inclination Variations

The inclination error also affects the overflight accuracy of two verification sites which must be maintained within ±1 km. The latitudes of both verification sites are ~35 deg N: the NASA site is on

11

Harvest Platform off Pt. Conception, Ca., the CNES site is near Lampedusa Island in the Mediterranean Sea. The variations in inclination cause an offset in the verification site overflight even if there is no difference between the actual and reference nodal crossings. The sensitivity of the site overflight longitude to variations in inclination is:

$$\frac{\partial L}{\partial i} = -\sin\phi_V \cos^2 L / \cos u_V$$

where L = longitude of verification site with respect to the ascending node

u_V = argument of latitude $(\omega + f)$ (2)

$\sin\phi_V = \sin u_V \sin i$

ϕ_V = latitude of the verification site

For the CNES verification site, $\partial L/\partial i = 74$ m/mdeg.

Eccentricity Vector and the Frozen Orbit

Following launch on 10 August 1992, a six-maneuver orbit acquisition sequence[19] lasting 42 days placed TOPEX/Poseidon in the operational orbit (Table 1), including achieving frozen orbit conditions. Use of a frozen orbit limits variations in the argument of periapse and eccentricity, resulting in reduced variability in orbital altitude for enhanced altimetry performance. Also, the frozen orbit eliminates the need for dedicated maneuvers to maintain these eccentricity vector (e,ω) parameters.

Frozen orbit conditions are realized through the balancing of the secular perturbations of the even zonal harmonics with the long-period perturbations of the odd zonal harmonics.[20] Physically, the frozen orbit is typically attributed to the cancellation of J_3 perturbations due to the earth's oblateness.[21-23] Deviations from this ideal steady state lead to closed curves in the (e,ω) phase plane. These curves can remain nearly closed even under the influence of non-gravitational perturbations such as drag and solar radiation pressure. For most frozen orbits, including TOPEX/Poseidon, the periapse is frozen at 90 deg,[24] and the eccentricity is very low (< 190 ppm).

The eccentricity vector conditions achieved by the orbit acquisition sequence were $e = 142.9$ ppm and $\omega = 90.6$ deg, compared to target values of $e = 95$ ppm and $\omega = 90$ deg (Table 1). The closed eccentricity vector contour shown in Fig. 17 describes the expected behavior when perturbed only by a 20x20 gravity field. This contour moves counterclockwise about the design point $\omega = 90$ deg and has a period of 26.74 months.[25] Observed values of (e,ω) shown in Fig. 17 have been separated into groups following each OMM. While these groups generally follow the expected counterclockwise movement of the frozen orbit, it is otherwise difficult to observe more detailed features which may be caused by each OMM, or attributable to perturbations other than earth gravity.
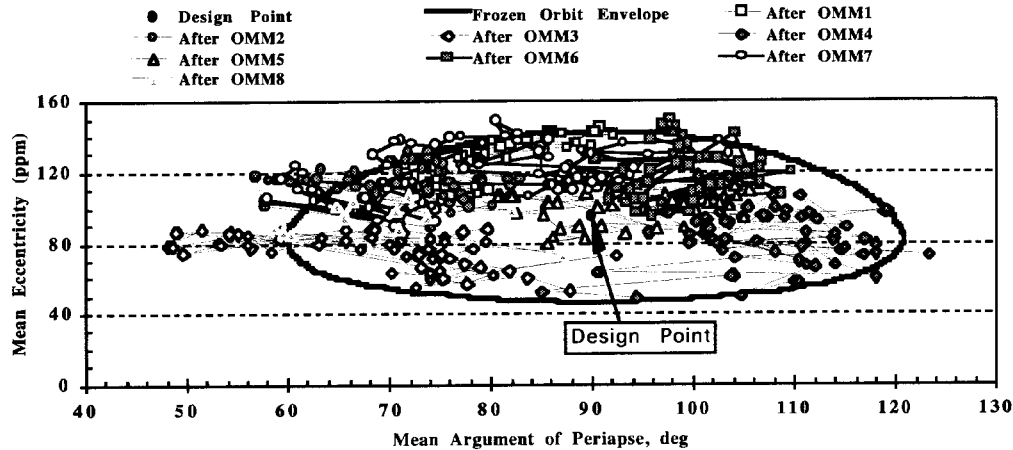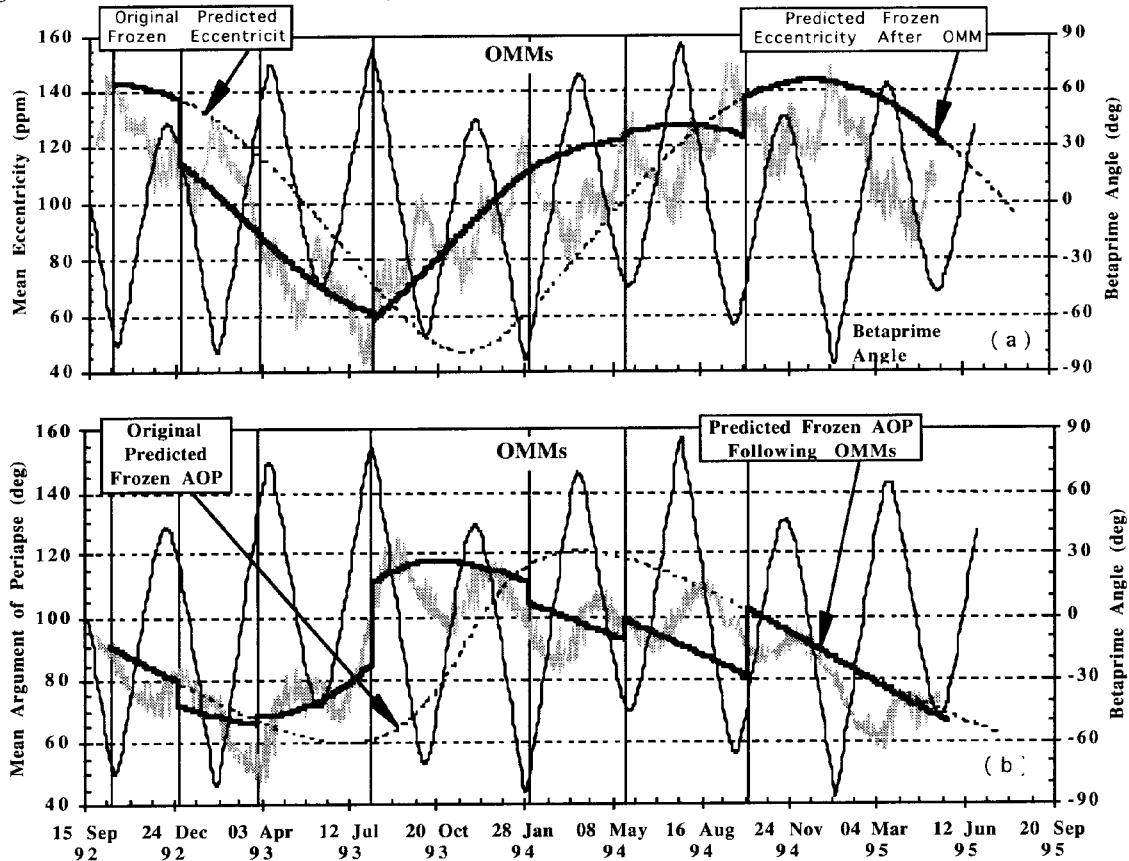

Fig. 17. Observed Eccentricity Vector (e,ω) Compared to the Predicted Frozen Orbit

The achieved mean eccentricity and argument of periapse are compared over time with the expected frozen values in Figs. 18(a) and (b), respectively. This examination reveals how the OMMs have affected

12

the observed e and ω variations.   Fig. 18(a) shows the observed mean eccentricity deviates from the original predicted frozen values. However, when the frozen predictions are updated following each OMM using current estimates of e and ω, the agreement with observations is considerably better. The same general behavior is evident for the argument of periapse (AOP) shown in Fig. 18(b).

Fig. 18. Effects of Maneuvers on the Eccentricity Vector (e, ω) Parameters
(a) Mean Eccentricity, and (b) Mean Argument of Periapse (AOP)

The maximum deviations of the observed (e,ω) values from the updated frozen predictions correlate very well with β' angle variations, as shown in Figs. 18(a,b). During periods of peak β' when the orbit is in full sun, the observed mean eccentricity is always less than the frozen value ($\beta' > 0$); this trend reverses when $\beta' < 0$. This behavior is caused by solar radiation pressure, as shown in Fig. 19 for the six-month period beginning 1 March 1994. For the three β' cycles included in this sample comparison, the mean eccentricity difference exhibits the same β'-dependent behavior. The argument of periapse exhibits maximum deviations from the updated frozen values near $\beta' = 0$ when solar radiation pressure has the greatest effect during the longest earth occultation intervals.

The frozen orbit has been maintained throughout the three-year prime mission without requiring dedicated maneuvers. However, every effort has been made to not increase the mean eccentricity when performing each OMM. While maneuver burns are constrained to occur over land to limit altimetry outages which could result from possible attitude disturbances, locations near an orbit node (usually mid-South America) have allowed mean eccentricity to be slightly reduced, or to remain unchanged. The two exceptions were following OMM4 and OMM8 executed near orbit periapse over northern Canada and eastern Russia, respectively, to satisfy satellite pointing constraints during turns to the burn attitude. These two maneuvers increased the post-maneuver values of the mean eccentricity, as shown in Fig. 18(a).
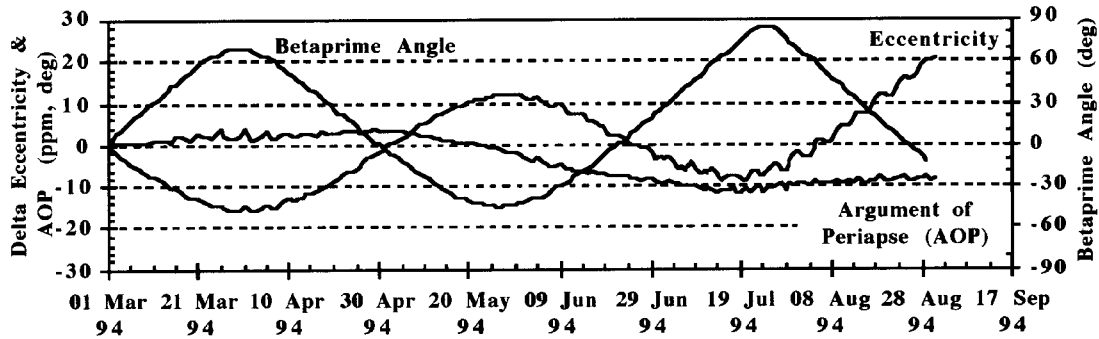
Fig. 19. Effects of Solar Radiation Pressure on Mean Eccentricity and Argument of Periapse

Variations in eccentricity (Δe) also affect equatorial crossings of the satellite ground track through variations in true anomaly (Δf). For a near-circular orbit $\Delta f = 2\Delta e$ sinM, where M is the mean anomaly.[17] A typical eccentricity error of ~10 ppm would cause a maximum $\Delta f = 2$ x 10^{-5} radians, equivalent to a equatorial crossing timing error $\Delta t = \Delta f/n \approx 22$ ms. The amplitude of the corresponding equatorial longitude error $\Delta \lambda = \omega_e \Delta t \approx 10$ m. This longitude error systematically oscillates with expected variations in the argument of periapse.

Ground Track History

As of 13 July 1995 the satellite had completed 13,116 orbits since first achieving the operational orbit on 23 September 1992. Of this total, only 95 ascending nodal crossings (~ 0.7%) have been outside the ±1-km ground track control band, and these violations were voluntary to provide additional analysis time to better characterize the behavior of the body-fixed forces before executing OMM1 on 12 October 1992. A total of seven additional OMMs have been executed since then, each designed to provide the maximum practical spacing between maneuvers. As can be seen from Fig. 20, the maneuver spacings have generally increased, the spacing between OMM7 and OMM8 being the largest at 228 days. Maneuver spacing and placement have sometimes been enhanced by modifying the nominal β' angle values governing entry into and out of the fixed yaw modes.[26] This strategy utilizes the large body-fixed forces during fixed yaw to alter the duration of orbital boost or deboost forces to slowly adjust the mean semimajor axis by the desired amount and thereby refine ground track motion.

Each maneuver has been executed as the ground track approaches the eastern control boundary after the mean semimajor axis had decayed below the reference value (see Fig. 6). The nominal strategy has been to execute each OMM at the next-to-last cycle boundary before the ground track would exit the eastern control boundary. This conservative practice provides an OMM backup opportunity still inside the control band, if for any reason the nominal maneuver does not occur as planned.

Distinct and important features in the ground track behavior are the oscillations during the western-most travel between each OMM. The precise nature of these oscillations depends on the complex combination of time-dependent influences of lunar and solar gravity, atmospheric drag, body-fixed forces, and the current value of the mean semimajor axis. The lunar and solar gravity influences become most prominent when the ground track drift rate slows when the mean semimajor axis is within a few meters of the reference value. Under these conditions third-body gravity forces cause the ground track to oscillate without significant net drift. This behavior is most prominent under low-drag conditions ($F_{10.7} \approx 80$), whereas the third-body perturbations can be somewhat masked when the drag level is higher ($F_{10.7} > 200$).

Summary

The TOPEX/Poseidon operational orbit and resulting ground track behavior have been analyzed and explained. All accuracy requirements have been met or surpassed. In particular, the operational orbit determination support provided by the GSFC/FDF using tracking data acquired via TDRSS surpasses requirements, due primarily to improved earth gravity modeling accuracy not reflected in pre-launch planning (Table 4). Mean orbital elements computed from FDF orbit determination solutions agree very well with values independently obtained from precision orbit determination results. These mean elements
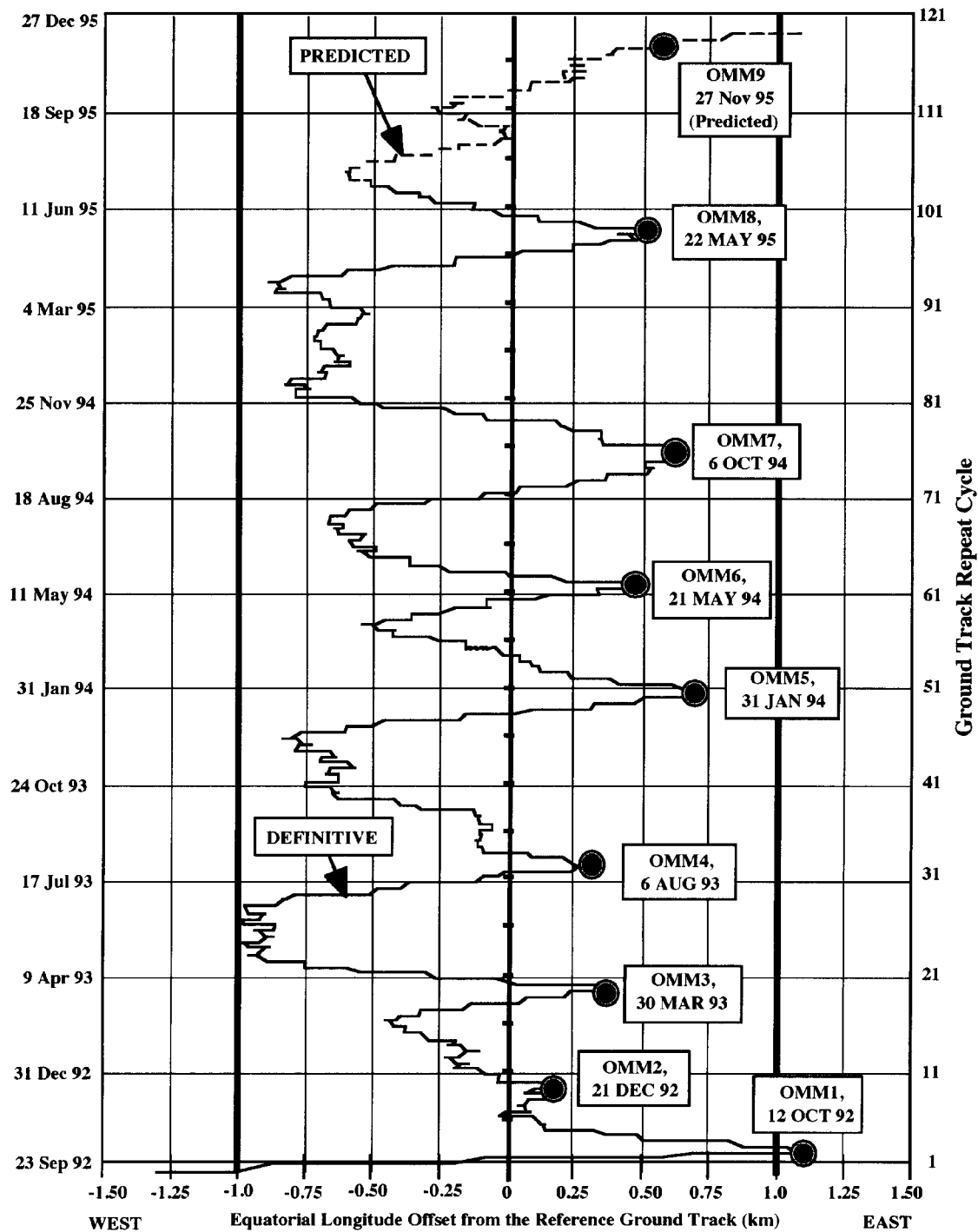
14

Fig. 20. TOPEX/Poseidon Ground Track History

15

were very accurately computed (Table 2) and demonstrated excellent stability. The three most important orbital parameters are the semimajor axis, inclination, and the eccentricity vector (e,ω). The analysis showed how semimajor axis must be adjusted to maintain ground track control, whereas the inclination and eccentricity vector do not require corrections.

Table 4. Comparison of Achieved Mean Element Accuracies with Pre-launch Requirements

Orbit Parameter	Reference Value	3σ Orbit Determination Requirement	Achieved OD Accuracy
Semimajor Axis a_o (km)	7714.42938	1 meter	< 5 cm
Inclination i_o (deg)	66.0408	1 mdeg	< 1 μdeg
Eccentricity e_o (ppm)	95	10 ppm	~0.01 ppm
Argument of Latitude at Node $\omega_o + f$ (deg)	0	5 mdeg	< 1 mdeg

$(\omega + f)$ is the argument of latitude, the sum of the argument of periapse and the true anomaly

The semimajor axis changes are caused by along-track forces induced primarily by the combined effects of atmospheric drag and body-fixed forces. Atmospheric drag always causes decay in semimajor axis, the rate mostly depends on the 81-day mean $F_{10.7}$ solar flux. The body-fixed forces can induce either boost or deboost in semimajor axis, the magnitude and direction depends on the satellite yaw control mode which systematically varies with the β' angle. Isolation of the drag contributions to semimajor axis behavior would permit reconstruction of atmospheric density from which improved density modeling might be feasible. However, confident separation of semimajor axis behavior into distinct contributions due to drag and body-fixed forces is prohibitive since both arise from along-track forces. Unfortunately, these forces cannot be separated without making certain assumptions about each force. It was shown that two representative density models, the JR and the DTM, provide consistent results. However, this result does not imply that either model is correct. The density modeling differences are of the same order as the estimation accuracy of the total once/rev non-gravitational accelerations provided by accurate quick-look laser-based orbit determination (~5 cm rms, radial position).[9] Since the total along-track accelerations are very small (on the order of one nanometer/s^2), opportunities for estimation accuracy improvements may be limited without adding tracking measurements with higher information content.[†] Also, it may become possible to improve the prediction model of the body-fixed forces as the understanding of the physical behavior improves.

The orbit inclination and eccentricity vector parameters have behaved as expected, and are expected to behave similarly during the three-year extended mission. The inclination exhibits periodic variations of ±3.8 mdeg about the reference value due almost entirely to lunar and solar gravitational perturbations. These deterministic perturbations have a significant effect on the satellite ground track, but are easily compensated for when adjusting the semimajor axis to control the ground track. The eccentricity vector provides a frozen orbit, limiting variations in the eccentricity and argument of periapse. Analysis showed distinct, albeit small, changes in eccentricity when OMMs were executed, even though the maneuver magnitudes were only 3 to 5 mm/s. Also, eccentricity variations on the order of ±20 ppm have been observed during orbit full sun ($\beta' > 55.7$ deg) due to solar radiation pressure.

Future orbit and ground track maintenance are expected to continue as before for the remainder of the TOPEX/Poseidon mission lifetime. Should the satellite remain operational for several more years, expected increases in solar activity as solar cycle 23 begins in early 1997 will increase the importance of atmospheric drag. As a result, the spacing between maneuvers may be as often as once every two to three months, compared to about twice annually during the current period of low solar activity.

References

1) TOPEX/Poseidon: Geophysical Evaluation, *Journal of Geophysical Research*, Vol. 99, Number C12, 15 December 1994.

2) Frautnick, J.C., Cutting, E., *Flight Path Design Issues for the TOPEX Mission*, AIAA-82-0202, AIAA 21st Aerospace Sciences Meeting, Orlando, Fl., January 1982.

[†] Recently, data acquired via the Global Positioning System (GPS) have been combined with laser data to fill coverage gaps, improving overall orbit determination accuracy.

16

3) Farless, D.L., *The Application of Periodic Orbits to TOPEX Mission Design*, AAS Paper 85-301, AAS/AIAA Astrodynamics Specialist Conference, Vail, Co., August 1985.

4) Guinn, J. R., *Periodic Gravitational Perturbations for Conversion Between Osculating and Mean Orbit Elements*, AAS Paper 91-430, AAS/AIAA Astrodynamics Specialists Conference, Durango, Co., August 1991.

5) Doll, C.E., Mistretta, G., Hart, R., *Accuracy Assessment of TDRSS-Based TOPEX/Poseidon Orbit Determination Solutions*, AAS 93-572, AAS/AIAA Astrodynamics Specialist Conference, Victoria, B.C., Canada, August 1993.

6) Bhat, R.S., Frauenholz, R.B., Cannell, P.E., *TOPEX/Poseidon Orbit Maintenance Maneuver Design*, AAS Paper 89-408, AAS/AIAA Astrodynamics Specialists Conference, Stowe, Vt., August 1989.

7) Frauenholz, R.B., Shapiro, B.E., *The Role of Predicted Solar Activity in TOPEX/Poseidon Orbit Maintenance Maneuver Design*, AAS Paper 91-515, AAS/AIAA Astrodynamics Specialists Conference, Durango, Co., August 1991.

8) Frauenholz, R.B., Hamilton, T.W., Shapiro, B.E., Bhat, R.S., *The Role of Anomalous Satellite-Fixed Accelerations in TOPEX/Poseidon Orbit Maintenance*, AAS Paper 93-570, AAS/AIAA Astrodynamics Specialists Conference, Victoria, B.C., Canada, August 1993.

9) Cangahuala, L.A., Christensen, E.J., Graat, E.J., Williams, B.G., Wolff, P.J., *TOPEX/Poseidon Precision Orbit Determination, 'Quick-Look' Operations and Orbit Verification*, AAS Paper 95-228, AAS/AIAA Spaceflight Mechanics Meeting, Albuquerque, New Mexico, February 1995.

10) Jacchia, L.G., *Static Diffusion Models of the Upper Atmosphere with Empirical Temperature Profiles*, Smithsonian Astrophysical Observatory Special Report 170, 30 December 1964.

11) Jacchia, L.G., *Atmosphere Models in the Region 110 to 2000 km*, in CIRA-72 COSPAR International Reference Atmosphere 1972, ed. The Committee for the COSPAR International; Reference Atmosphere (CIRA) of COSPAR (Committee on Space Research) Working Group 4, Akadamie-Verlkag, Berlin, 1972.

12) Jacchia, L.G., *Thermospheric Temperature, Density, and Composition: New Models*, Smithsonian Astrophysical Observatory Special Report 375, 15 March 1977.

13) Roberts, Charles, *An Analytic Model for Upper Atmosphere Densities Based Upon Jacchia's 1970 Models*, Celestial Mechanics 4(1971), 368-377.

14) Barlier, F., Berger, C., Falin, J.L., Kockarts, G., and Thuillier, G., *Comparisons Between Various Semi-empirical Thermospheric Models of the Terrestrial Atmosphere*, Belgisch Instituut voor Ruimte-Aeronomie, 1979.

15) Richter, Robert, *Radiation Forces Acting on the TOPEX/Poseidon Spacecraft Along the Velocity Vector due to the Solar Array - Initial Results*, JPL IOM 3544-TOP-93-004, 8 July 1993 (internal document).

16) Richter, Robert, *Determination of Satellite Acceleration*, JPL IOM 3544-TOP-93-007, 1 September 1993 (internal document).

17) Richter, Robert, *Radiation Forces during Sinusoidal Yaw Steering for Three Solar Array Bias Angles*, JPL IOM 3544-TOP-93-014, 12 November 1993 (internal document).

18) Bhat, R. S., and Cannell, P. E., *Effects of Variation of Mean Orbital Parameters on Ground Track Pattern and Repeatability*, JPL IOM 314.5-1330, 26 January 1989 (internal document).

19) Bhat, R.S., Shapiro, B.E., Frauenholz, R.B., *TOPEX/Poseidon Orbit Acquisition Maneuver Sequence*, AAS Paper 93-571, AAS/AIAA Astrodynamics Specialists Conference, Victoria, B.C., Canada, August 1993.

20) Chobotov, Vladimir A., *Orbital Mechanics*, AIAA Education Series, ISBN 1-56347-007-1, 1991.

21) Nickerson, K.G, Herder, R.W, Glass, A.B., Cooley, J.L, "Application of Altitude Control Techniques for Low Altitude Earth Satellites, *Journal of the Astronautical Sciences*, XXVI, 2, pp. 129-148, April-June 1978.

22) Cutting, E., Born, G.H., and Frautnick, J.C., Orbit Analysis for SEASAT-A, *Journal of the Astronautical Sciences*, XXVI, 4, pp. 315-342, Oct-Dec, 1978.

23) Herder, R.W., Cullen, M.F., Glass, A.B., *Description and Application of the Frozen Orbit Concept*, Computer Sciences Corporation, CSC/TM-79/6089, 1979.

24) Smith, J.C., *Analysis and Application of Frozen Orbits for the TOPEX Mission*, AIAA-86-2069-CP, AIAA/AAS Astrodynamics Conference, Williamsburg, VA., August 1986.

25) Shapiro, Bruce, *Phase Plane Analysis and Observed Frozen Orbit for the TOPEX/Poseidon Mission*, submitted to Sixth International Space Conference of Pacific Basin Societies, Marina del Rey, CA, 6-8 December 1995.

26) Shapiro, Bruce E., Bhat, Ramachandra S., Frauenholz, Raymond B., *Using Anomalous Along-Track Forces to Control the TOPEX/Poseidon Ground Track*, AAS 94-165, AAS/AIAA Spaceflight Mechanics Meeting, Cocoa Beach, Fl., February 1994.